SUPPORTING INFORMATION

van der Waals Contact between Nucleophile and Transferring Phosphorus Is Insufficient To Achieve Enzyme Transition-State Architecture

Luke A. Johnson,[†,¶,#] Angus J. Robertson,[†,#] Nicola J. Baxter,[†,‡] Clare R. Trevitt,[†] Claudine Bisson,[†,§] Yi Jin,[†,¶] Henry P. Wood,[†] Andrea M. Hounslow,[†] Matthew J. Cliff,[‡] G. Michael Blackburn,[†] Matthew W. Bowler,[‖] and Jonathan P. Waltho,*[,†,‡]

[†] Krebs Institute for Biomolecular Research, Department of Molecular Biology and Biotechnology, The University of Sheffield, Sheffield, S10 2TN, United Kingdom

[‡] Manchester Institute of Biotechnology and School of Chemistry, The University of Manchester, Manchester, M1 7DN, United Kingdom

[‖] European Molecular Biology Laboratory, Grenoble Outstation, 71 avenue des Martyrs, CS 90181 F-38042 Grenoble, France

[#] (L.A.J. and A.J.R.) These authors contributed equally

[¶] (L.A.J. and Y.J.) School of Chemistry, Cardiff University, Cardiff, CF10 3AT, United Kingdom

[§] (C.B.) Institute of Structural and Molecular Biology, Department of Biological Sciences, Birkbeck, University of London, London, WC1E 7HX, United Kingdom

* E-mail for J.P.W.: j.waltho@sheffield.ac.uk

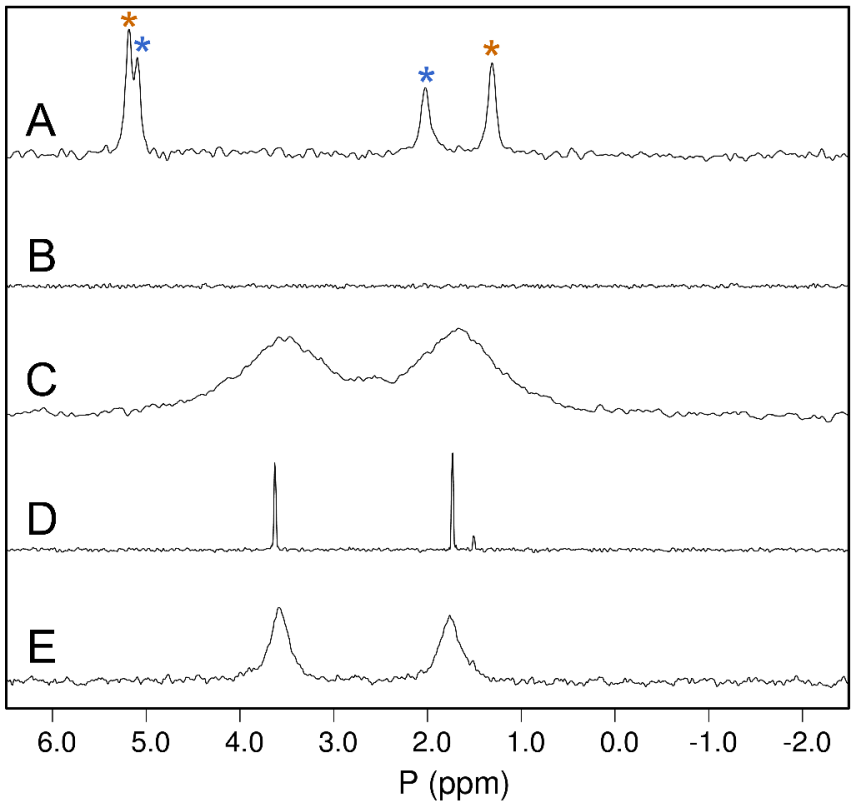
A
B
C
D
E
6.0
5.0
4.0
3.0
2.0
1.0
0.0
-1.0
-2.0
P (ppm)

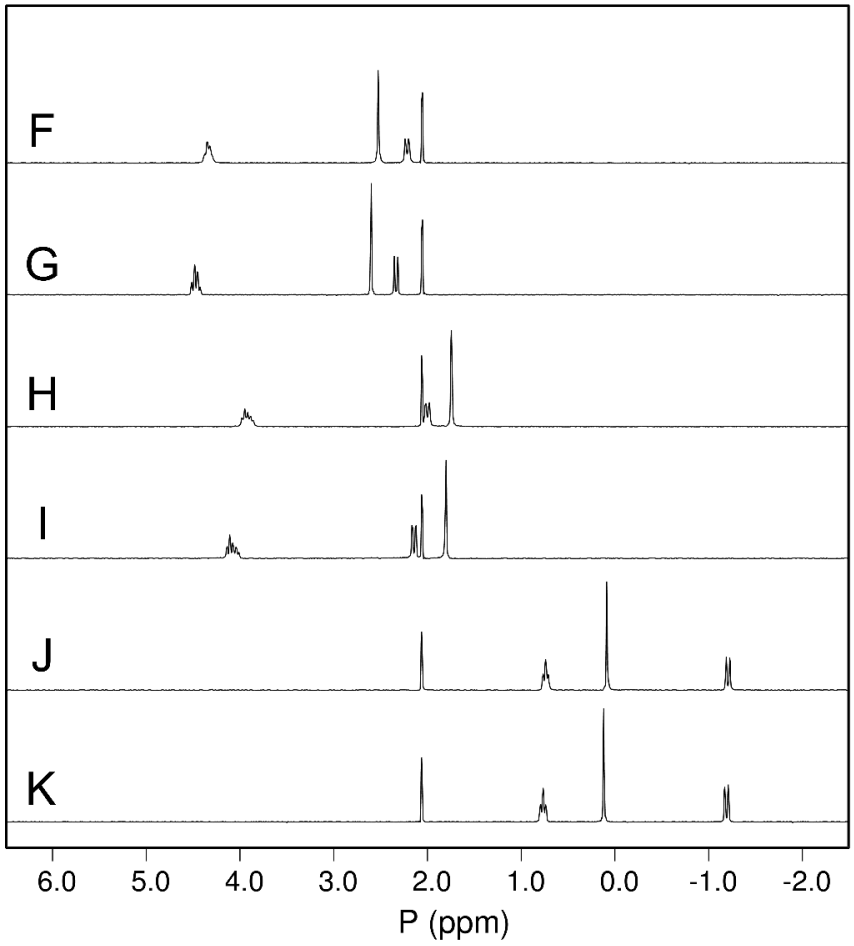
F
G
H
I
J
K
6.0
5.0
4.0
3.0
2.0
1.0
0.0
-1.0
-2.0
P (ppm)

Figure S1. ^{31}P NMR spectra illustrating steps in the purification of βPGM_{D10N} and βG16BP, together with the dependence of G6P and βG1P chemical shifts on pH and Mg^{II} concentration. (A – E) Samples were prepared in standard NMR buffer and spectra were acquired typically with 10000 transients over 50 ppm using proton-phosphorus decoupling. (A) βPGM_{D10N} immediately following purification showing four ^{31}P resonances consistent with the population of two tight noncovalently bound βPGM_{D10N}:βG16BP complexes. The orange asterisks indicate ^{31}P peaks from the 6-phosphate (5.17 ppm) and the 1-phosphate (1.30 ppm) groups of βG16BP in the Mg^{II}-bound βPGM_{D10N}:P1G6P complex and the blue asterisks indicate ^{31}P peaks from the 6-phosphate (5.08 ppm) and the 1-phosphate (2.01 ppm) groups of βG16BP in the Mg^{II}-free βPGM_{D10N}:P1G6P complex. (B) Substrate-free βPGM_{D10N} generated by unfolding the βPGM_{D10N}:βG16BP complexes in 4 M guanidine hydrochloride, with 200-fold dilution of the ligand using buffer exchange, and subsequent refolding of βPGM_{D10N} to a native conformation. The absence of ^{31}P resonances indicates that βG16BP no longer occupies the active site. (C) βG16BP extracted by membrane filtration from heat denatured (2 min at 80 °C) βPGM_{D10N}:βG16BP complexes. The two ^{31}P resonances are broadened significantly due to exchange of coordination between the phosphate groups of βG16BP and Mg^{II} ions present in the sample. (D) Addition of 6 mM EDTA to the sample in (C) chelates the Mg^{II} ions resulting in a significant narrowing of linewidths for the two ^{31}P peaks (3.63 and 1.74 ppm). This sample was used to record the $^{1}H^{13}C$ HSQC spectrum shown in Figure S2B. (E) Chemically synthesized βG16BP (Prof. Nicholas Williams, Department of Chemistry, The University of Sheffield) in standard NMR buffer. Correspondence in chemical shift values between the two ^{31}P resonances (C – E) is consistent with βG16BP being isolated from the βPGM_{D10N}:βG16BP complexes. (F – K) Samples contained 10 mM G6P, 10 mM βG1P and 20 mM sodium phosphate in 10 mM Tris and 10 mM sodium acetate buffer at (F and G) pH 9.0, (H and I) pH 7.0 and (J and K) pH 4.0, containing either (F, H, J) 10 mM $MgCl_2$ or (G, I, K) no Mg^{II}. A capillary containing 200 mM sodium phosphate at pH* 7.2 in 100% $^{2}H_2O$ was included in the sample as a chemical shift reference (2.06 ppm) and for the deuterium lock. Other resonances are assigned as follows: G6P (left hand multiplet), inorganic phosphate (singlet) and βG1P (right hand doublet). Spectra were acquired with 256 transients over 50 ppm and without proton-phosphorus decoupling to differentiate the G6P and βG1P resonances.

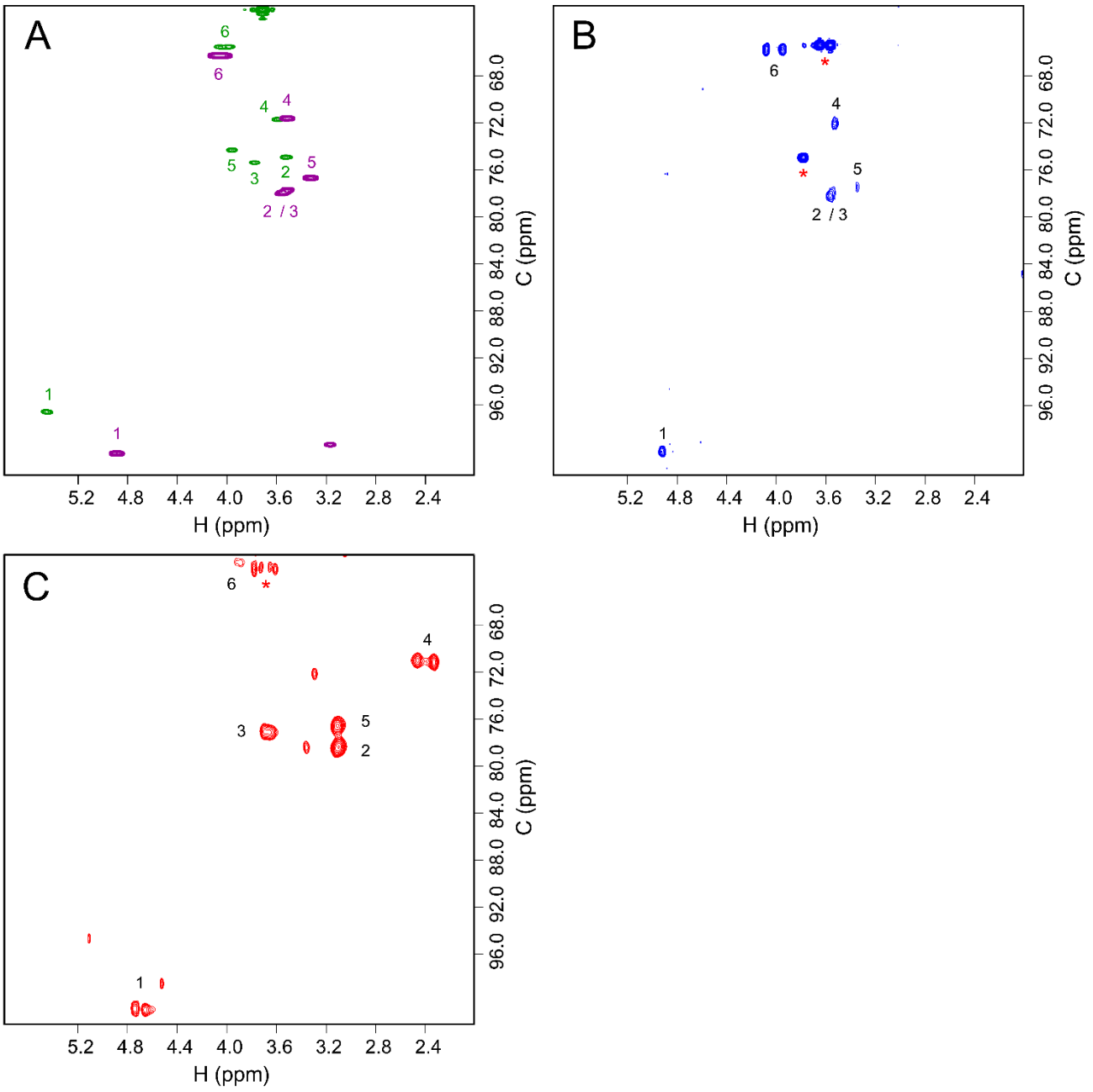

Figure S2. Assigned $^{1}H^{13}C$ HSQC spectra of glucose 1,6-bisphosphate species. (A) Commercially produced αG16BP (Sigma) in 100% $^{2}H_2O$ (green) and chemically synthesized βG16BP in 100% $^{2}H_2O$ (magenta). (B) βG16BP extracted by membrane filtration from heat denatured (2 min at 80 °C) βPGM_{D10N}:βG16BP complexes in standard NMR buffer containing 6 mM EDTA. The red asterisks denote peaks arising from the buffer. (C) Uniformly ^{13}C-labeled βG16BP in the Mg^{II}-bound βPGM_{D10N}:P1G6P and Mg^{II}-free βPGM_{D10N}:P1G6P complexes in standard NMR buffer.

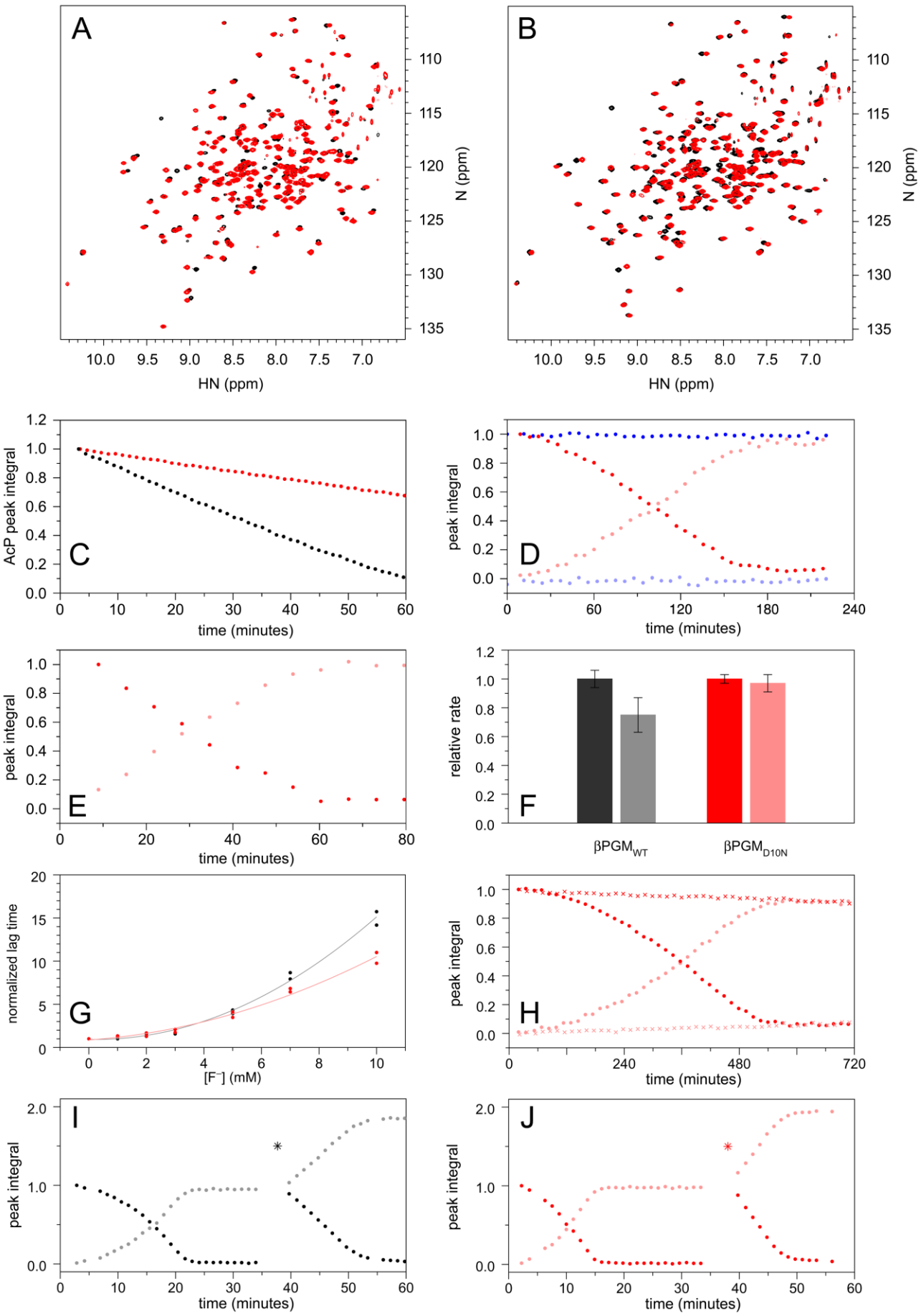
A
B
110
115
120
125
130
135
N (ppm)
10.0
9.5
9.0
8.5
8.0
7.5
7.0
HN (ppm)
C
AcP peak integral
time (minutes)
D
peak integral
E
F
relative rate
βPGM$_{WT}$
βPGM$_{D10N}$
G
normalized lag time
[F$^-$] (mM)
H
I
J

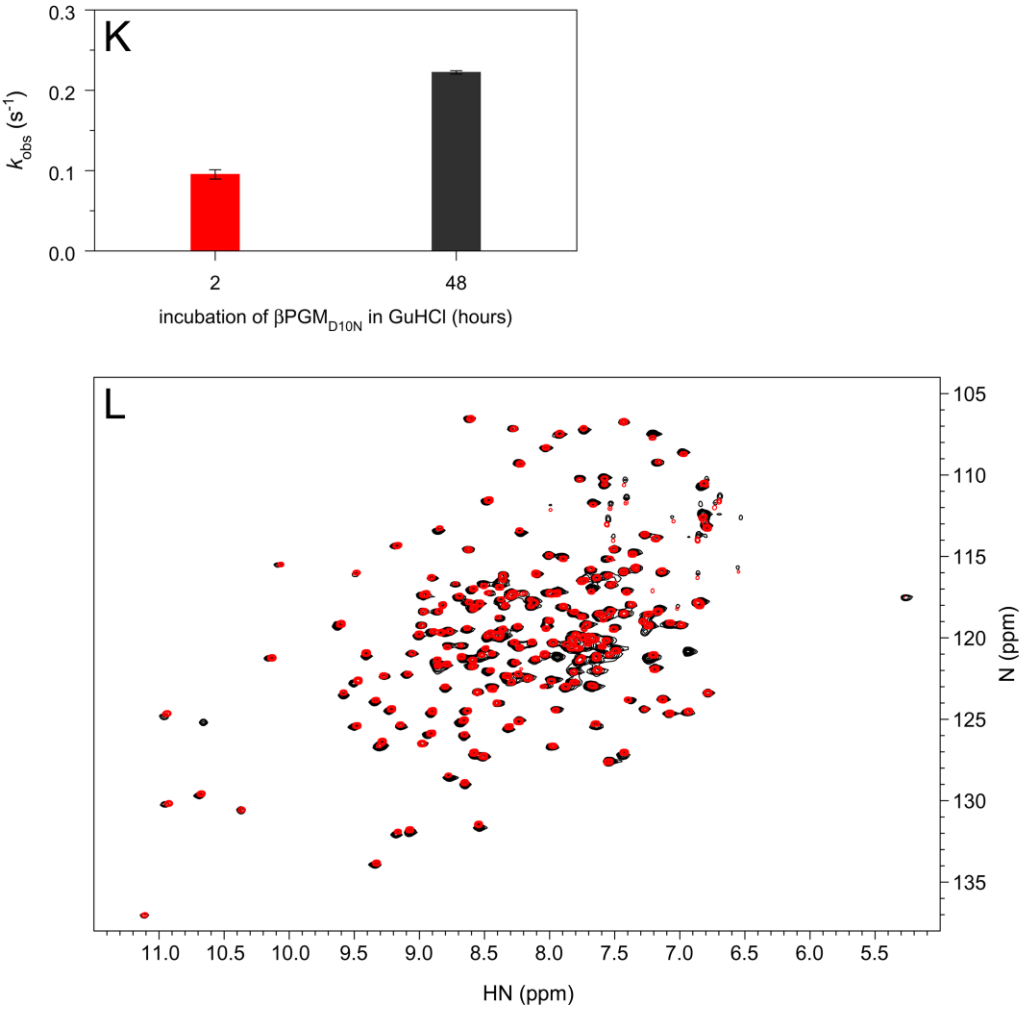

Figure S3. Comparison of $^{1}H^{15}N$ TROSY spectra, acetyl phosphate (AcP) hydrolysis kinetics, inhibition of βPGM$_{WT}$ and βPGM$_{D10N}$ by inorganic phosphate and fluoride, and βG1P equilibration by βPGM$_{D10N}$, βPGM$_{D8N}$ and the reconstituted βPGM$_{D10N}$:βG16BP complexes. (A) Superposed $^{1}H^{15}N$ TROSY spectra of (black) βPGM$_{WT}$ and (red) substrate-free βPGM$_{D10N}$, generated by unfolding the copurified βPGM$_{D10N}$:βG16BP complexes in 4 M guanidine hydrochloride, with 200-fold dilution of the ligand using buffer exchange, and subsequent refolding to a native conformation. Samples typically contained either 0.5 mM βPGM$_{WT}$ or 0.5 mM substrate-free βPGM$_{D10N}$ in standard NMR buffer with 50 mM $MgCl_2$. (B) Superposed $^{1}H^{15}N$ TROSY spectra of (black) βPGM$_{WT}$:BeF_3 complex and (red) βPGM$_{D10N}$:BeF_3 complex. The complexes containing the BeF_3^- moiety coordinated at D8 are structural mimics of βPGM$_{WT}^{P}$ and βPGM$_{D10N}^{P}$ and were generated from samples typically containing either 0.5 mM βPGM$_{WT}$ or 0.5 mM substrate-free βPGM$_{D10N}$ in standard NMR buffer with 5 mM $BeCl_2$ and 10 mM NH_4F. (C) Hydrolysis kinetics of AcP to inorganic phosphate and acetate

by (black) βPGM_{WT} and (red) substrate-free βPGM_{D10N}, monitored by ^{31}P NMR spectra with integration of the AcP peak as a function of time. The samples contained either 250 μM βPGM_{WT} or 250 μM substrate-free βPGM_{D10N}, together with 50 mM AcP in standard kinetic buffer containing 50 mM $MgCl_2$ and 1 mM EDTA. Hydrolysis rate constants were obtained from linear fitting of the data (βPGM_{WT} = 0.06 ± 0.006 s^{-1}; βPGM_{D10N} = 0.02 ± 0.002 s^{-1}). A control experiment involving 50 mM AcP alone in standard kinetic buffer established that hydrolysis of AcP was insignificant over the same time frame. (D) Reaction kinetics of (red / pink) substrate-free βPGM_{D10N} (5 μM) and (blue / light blue) βPGM_{D8N} (10 μM) for the equilibration of 10 mM βG1P with G6P in the presence of 20 mM AcP monitored by ^{31}P NMR spectra using normalized integral values of (red / blue) the βG1P peak and (pink / light blue) the G6P peak as a function of time. (E) Reaction kinetics of substrate-free βPGM_{D10N} (5 μM) for the equilibration of 10 mM βG1P with G6P in the presence of βG16BP (extracted from the copurified βPGM_{D10N}:βG16BP complexes) monitored by ^{31}P NMR spectra using normalized integral values of (red) the βG1P peak and (pink) the G6P peak as a function of time. (F) Relative reaction rates monitored by ^{31}P NMR spectra of βPGM_{WT} (0.1 – 0.25 μM; n = 3) and substrate-free βPGM_{D10N} (45 μM; n = 3) for the equilibration of 10 mM βG1P with G6P in the presence of 20 mM AcP in (dark gray / red) the standard kinetic buffer and (light gray / pink) with the addition of 20 mM sodium phosphate. (G) Reaction kinetics monitored by the glucose 6-phosphate dehydrogenase coupled assay of βPGM_{WT} (5 nM) and substrate-free βPGM_{D10N} (500 nM) for the equilibration of 10 mM βG1P with G6P in the presence of 20 mM AcP in the standard kinetic buffer with increasing concentrations of fluoride (0, 1, 2, 3, 5, 7 and 10 mM). Time points corresponding to the end of the lag phase (as measured by first derivative analysis) for each of the fluoride concentrations were normalized against data recorded in the absence of fluoride. (H) Reaction kinetics of the reconstituted βPGM_{D10N}:βG16BP complexes (2.5 μM) for the equilibration of 10 mM βG1P with G6P in the (crosses) absence and (circles) presence of 20 mM AcP monitored by ^{31}P NMR spectra using normalized integral values of (red) the βG1P peak and (pink) the G6P peak as a function of time. (I and J) Reaction kinetics of (black / gray) βPGM_{WT} (0.25 μM) and (red / pink) substrate-free βPGM_{D10N} (45 μM) for the equilibration of 10 mM βG1P with G6P in the presence of 20 mM AcP monitored by ^{31}P NMR spectra using normalized integral values of the βG1P peak (black / red) and G6P peak (gray / pink) as a function of time. Asterisks denote the time points at which samples were recharged with additional 10 mM βG1P. Missing ^{31}P data at ca. 5 and 55 minutes in the time courses is to allow for the acquisition of ^{1}H NMR spectra. A k_{cat} of 0.2 ± 0.08 s^{-1} (n = 8) was derived for βPGM_{D10N} from the linear segment of the first kinetic profile, compared with 70 ± 30 s^{-1} (n = 7)

for βPGM_{WT}. Note that for the reaction kinetics monitored by ^{31}P NMR spectra, the enzyme concentration was adjusted to allow for similar signal-to-noise ratios to be obtained on the different spectrometers used. (K) Observed catalytic rate constants (k_{obs}) monitored by the glucose 6-phosphate dehydrogenase coupled assay of βPGM_{D10N} (500 nM) for the equilibration of 230 μM βG1P with G6P in the presence of 10 mM AcP for (red) substrate-free βPGM_{D10N} following ca. 2 h incubation with 4 M guanidine hydrochloride and (black) substrate-free βPGM_{D10N} following ca. 48 h incubation with 4 M guanidine hydrochloride in the unfolding-dilution-refolding procedure. (L) Superposed $^{1}H^{15}N$ TROSY spectra of the reconstituted Mg^{II}-bound βPGM_{D10N}:P1G6P complex in standard NMR buffer containing 50 mM $MgCl_2$, 20 mM AcP and 10 mM G6P with (red) substrate-free βPGM_{D10N} following ca. 2 h incubation with 4 M guanidine hydrochloride and (black) substrate-free βPGM_{D10N} following ca. 48 h incubation with 4 M guanidine hydrochloride in the unfolding-dilution-refolding procedure.

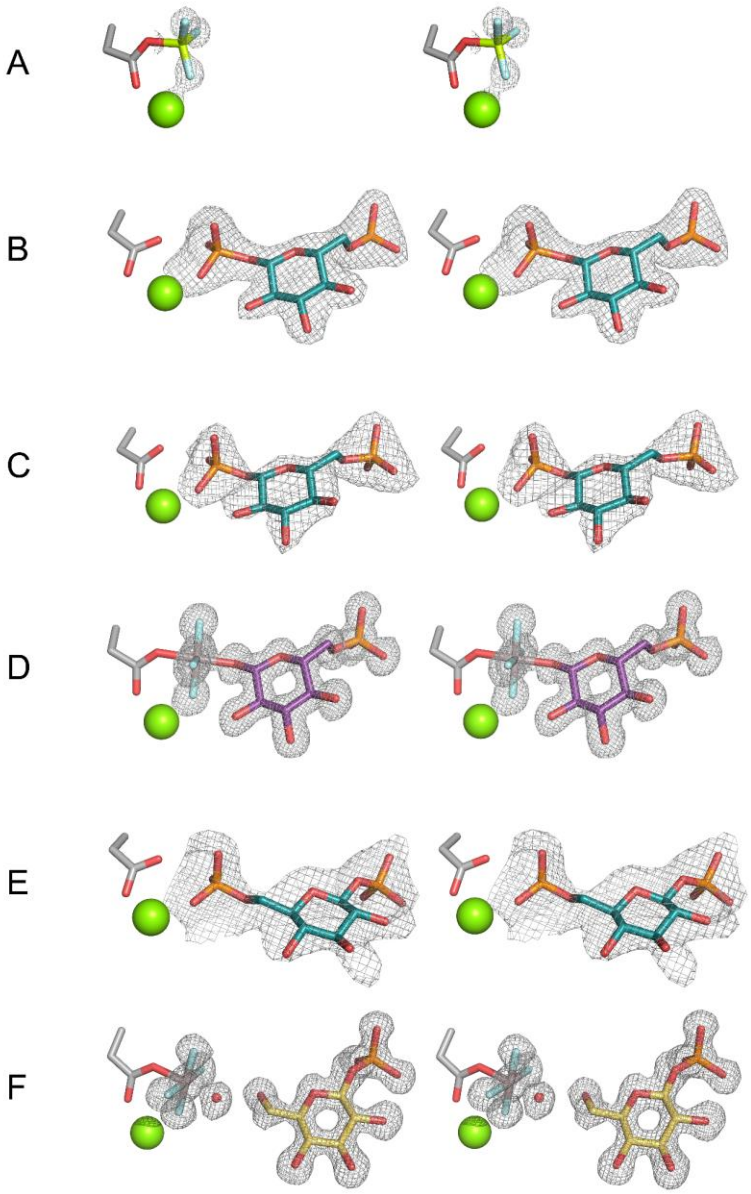

Figure S4. Stereoviews of difference density (Fo – Fc) for the βPGM$_{D10N}$ complexes. The active sites of (A) βPGM$_{D10N}$:BeF_3 complex (PDB 5OJZ), (B) βPGM$_{D10N}$:P1G6P complex (PDB 5OK1), (C) copurified βPGM$_{D10N}$:P1G6P complex (PDB 5O6P), (D) βPGM$_{D10N}$:AlF_4:G6P complex (PDB 5OK2), (E) βPGM$_{D10N}$:P6G1P complex (PDB 5OK0) and (F) βPGM$_{D10N}$:AlF_4:H_2O:βG1P complex (PDB 5O6R). The side chain of D8 and active site ligands are shown as sticks in standard CPK colors, with beryllium (light green), fluorine (light blue), aluminum (dark gray), βG16BP (teal carbon atoms), G6P (purple carbon atoms) and βG1P (gold carbon atoms). An axially coordinated water (red) and the catalytic Mg^{II} ion (green) are drawn as spheres. Difference density (Fo – Fc; gray mesh) was generated following ligand omission from the final structures, and is contoured selectively at 2.5σ (E) and 3σ (A–D, F) for the BeF_3^-, βG16BP, AlF_4^-, G6P, βG1P and water ligands.

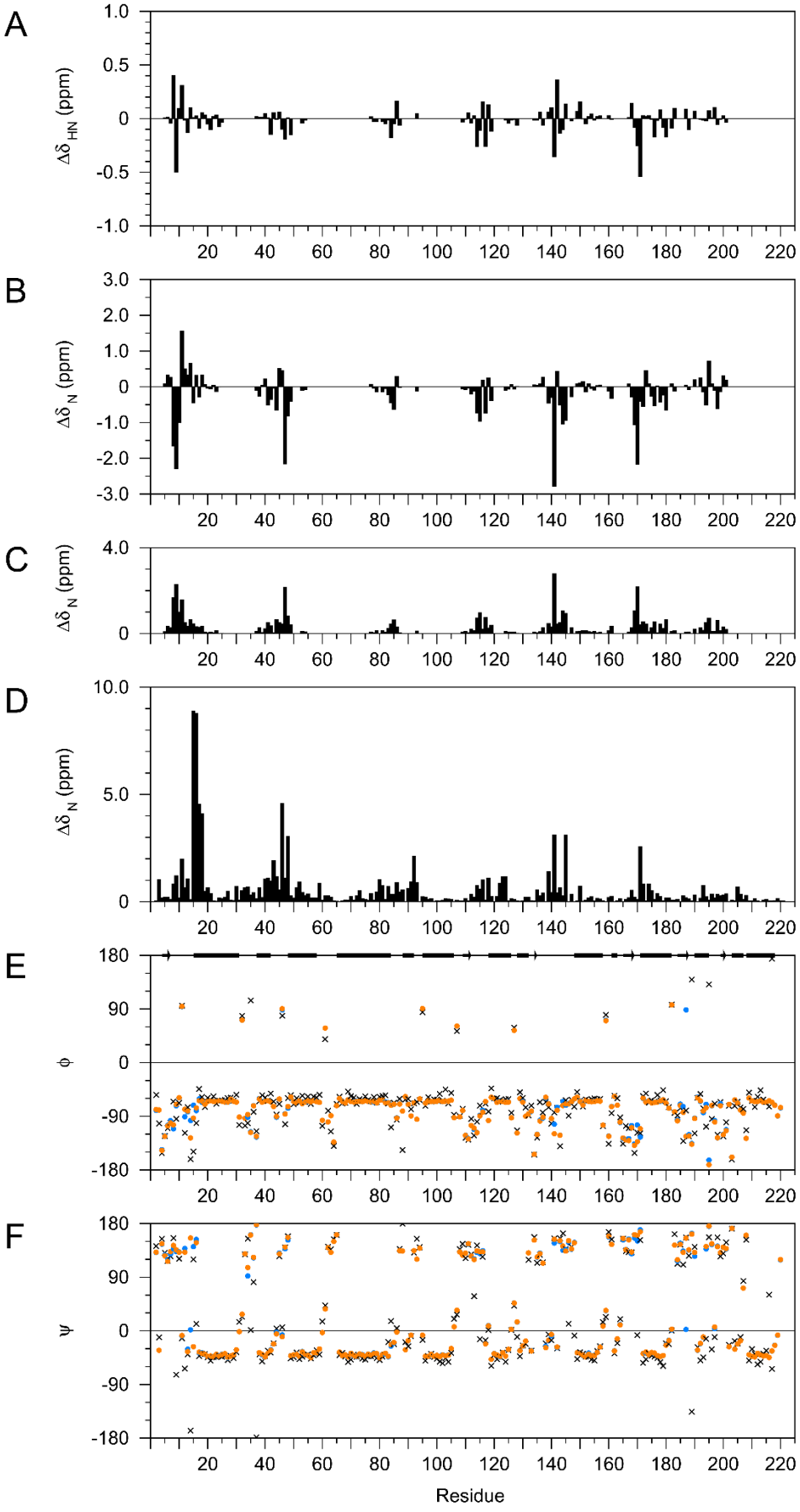
A
B
C
D
E
F
Δδ HN (ppm)
Δδ N (ppm)
Δδ N (ppm)
Δδ N (ppm)
ϕ
ψ
Residue

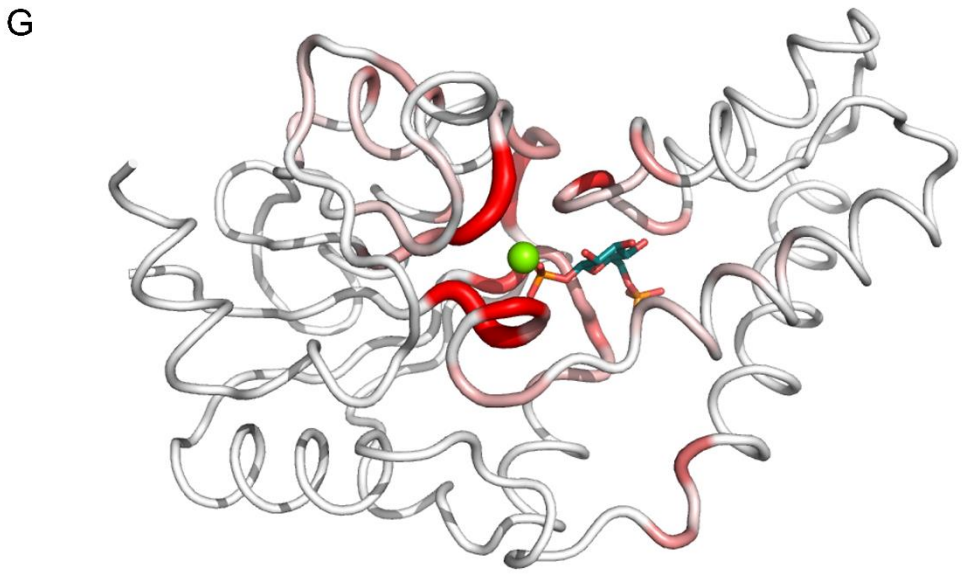

Figure S5. Chemical shift analysis of the Mg^{II}-bound βPGM_{D10N}:P1G6P and the Mg^{II}-free βPGM_{D10N}:P1G6P complexes. Histograms of residue specific chemical shift changes for the βPGM_{D10N}:P1G6P complexes calculated as $\Delta\delta = \delta_{Mg\text{-}bound} - \delta_{Mg\text{-}free}$ for (A) backbone H_N atoms, (B) backbone N atoms and (C) as $\Delta\delta = [(\delta_{Mg\text{-}bound} - \delta_{Mg\text{-}free})^2]^{1/2}$ for the backbone N atoms. (D) Residue specific chemical shift changes between the Mg^{II}-bound βPGM_{D10N}:P1G6P complex and the βPGM_{WT}:MgF_3:G6P TSA complex (BMRB 7234)[20] calculated as $\Delta\delta = [(\delta_{\beta PGM\text{-}D10N\text{-}P1G6P} - \delta_{\beta PGM\text{-}WT\text{-}TSA})^2]^{1/2}$ for the backbone N atoms. The data have been plotted with the same vertical scaling as (C) so that the size of $\Delta\delta_N$ can be compared. (E and F) Backbone dihedral angle prediction of βPGM_{D10N} in the Mg^{II}-bound βPGM_{D10N}:P1G6P complex (orange circles) and the Mg^{II}-free βPGM_{D10N}:P1G6P complex (blue circles) obtained with TALOS-N[55] using the backbone ^1H_N, ^{15}N, $^{13}C\alpha$, $^{13}C\beta$ and $^{13}C'$ chemical shifts. For comparison, backbone dihedral angles were extracted from the βPGM_{D10N}:P1G6P crystal structure (PDB 5OK1) and are shown as black crosses. Secondary structure elements from βPGM_{WT} (PDB 2WHE)[20] are indicated by bars (α-helices) and arrows (β-strands) at the top of the panel. (G) Structure of the βPGM_{D10N}:P1G6P complex (PDB 5OK1) with residues colored according chemical shift changes calculated as $\Delta\delta = [\Delta\delta_{HN}^2 + (0.12 \times \Delta\delta_N)^2]^{1/2}$, between the Mg^{II}-bound βPGM_{D10N}:P1G6P complex and the Mg^{II}-free βPGM_{D10N}:P1G6P complex, with the intensity of color and thickness of the backbone corresponding to larger Δδ values. The βG16BP ligand is shown as CPK-colored sticks and the catalytic Mg^{II} ion is indicated as a green sphere.

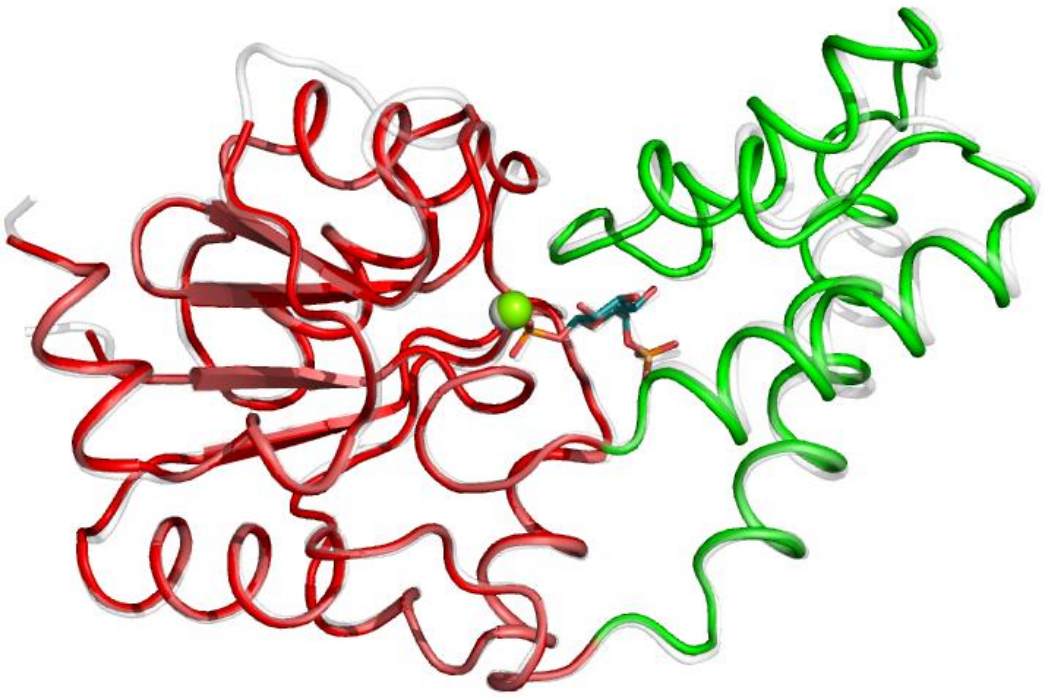

Figure S6. Comparison of the two crystal structures of the βPGM_{D10N}:P1G6P complex. The reconstituted βPGM_{D10N}:P1G6P complex (PDB 5OK1; pale gray ribbon) and the copurified βPGM_{D10N}:P1G6P complex (PDB 5O6P; red and green ribbon) have been superposed on the core domains (left). The βG16BP ligands are drawn as sticks (in CPK colors for PDB 5O6P) and the catalytic Mg^{II} ions are shown as spheres (green sphere for PDB 5O6P).

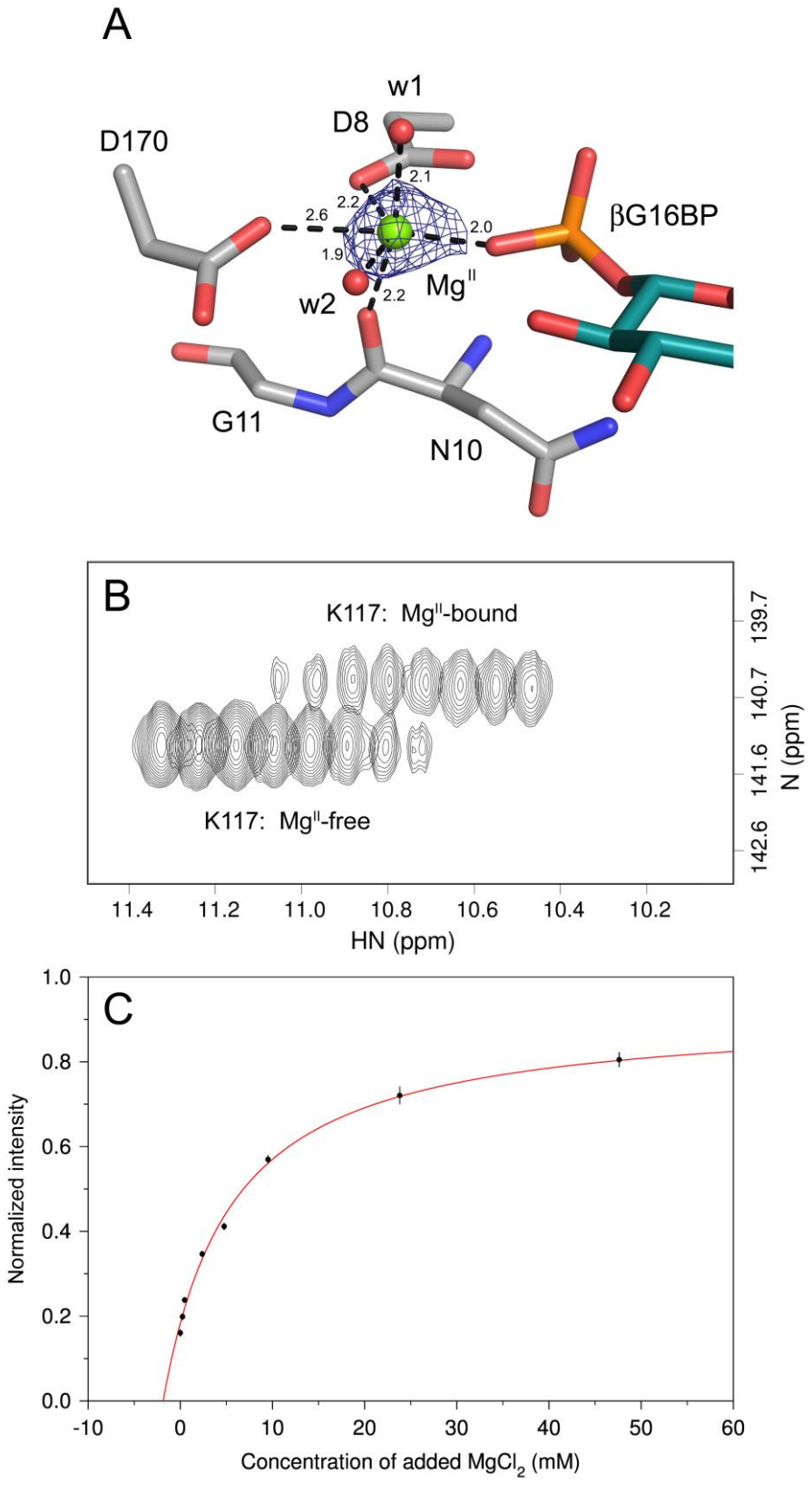
A
w1
D8
D170
2.1
2.2
2.6
2.0
βG16BP
1.9
Mg^II
w2
2.2
G11
N10
B
K117: Mg^II-bound
K117: Mg^II-free
139.7
140.7
141.6
142.6
N (ppm)
11.4
11.2
11.0
10.8
10.6
10.4
10.2
HN (ppm)
C
1.0
0.8
0.6
0.4
0.2
0.0
Normalized intensity
-10
0
10
20
30
40
50
60
Concentration of added MgCl2 (mM)

Figure S7. Coordination and binding affinity of the catalytic Mg^{II} ion in the βPGM_{D10N}:P1G6P complex. (A) Active site of the βPGM_{D10N}:P1G6P complex (PDB 5OK1) with βG16BP and selected residues shown as CPK-colored sticks, structural waters shown as red spheres and the catalytic Mg^{II} ion indicated as a green sphere. The asymmetrical 2Fo – Fc electron density for the catalytic Mg^{II} ion is contoured at 2.5σ (blue mesh), with Mg^{II} coordination (black dashes) and atomic distances (Å) indicated. Restrained refinement of the βPGM_{D10N}:P1G6P complex (1.9 Å) results in a suboptimal coordination geometry for the catalytic Mg^{II} ion, as the cumulative atomic distance is ~0.2 Å too long between the oxygen atom of the 1-phosphate group of βG16BP (O – Mg^{II} = 2.0 Å) and the side chain carboxylate Oδ1 atom of D170 (O – Mg^{II} = 2.6 Å). The locations of the side chain carboxylate group of D8, the backbone carbonyl group of N10 and the water molecules present suggest that a more optimal binding geometry is accessible for the Mg^{II} ion when centered ~0.2 Å further towards the side chain carboxylate Oδ1 atom of D170. (B) Changes in peak intensity for residue K117 in a superposed series of $^{1}H^{15}N$ TROSY spectra (offset in ^{1}H frequency for clarity) as $MgCl_2$ is titrated into the Mg^{II}-free βPGM_{D10N}:P1G6P complex. As the concentration of $MgCl_2$ increases (left to right), the population of the Mg^{II}-free βPGM_{D10N}:P1G6P complex decreases with a concomitant increase in the population of the Mg^{II}-bound βPGM_{D10N}:P1G6P complex, consistent with a slow conformational exchange on the NMR time scale. The slow rate of Mg^{II} exchange most likely reflects the exclusion of its binding site by βG16BP. (C) Calculation of the binding affinity of Mg^{II} for the Mg^{II}-free βPGM_{D10N}:P1G6P complex using nonlinear least-squares fitting (red line) of normalized changes in averaged $^{1}H^{15}N$ TROSY peak intensities (black circles) for residues N10, G11, A115, K117 and I150. The dissociation constant (K_d) was determined to be 7.1 ± 0.6 mM. The initial concentration of Mg^{II} in the solution was evaluated as 1.9 ± 0.1 mM. Errors in peak intensity measurements are indicated as vertical black lines on each data point.

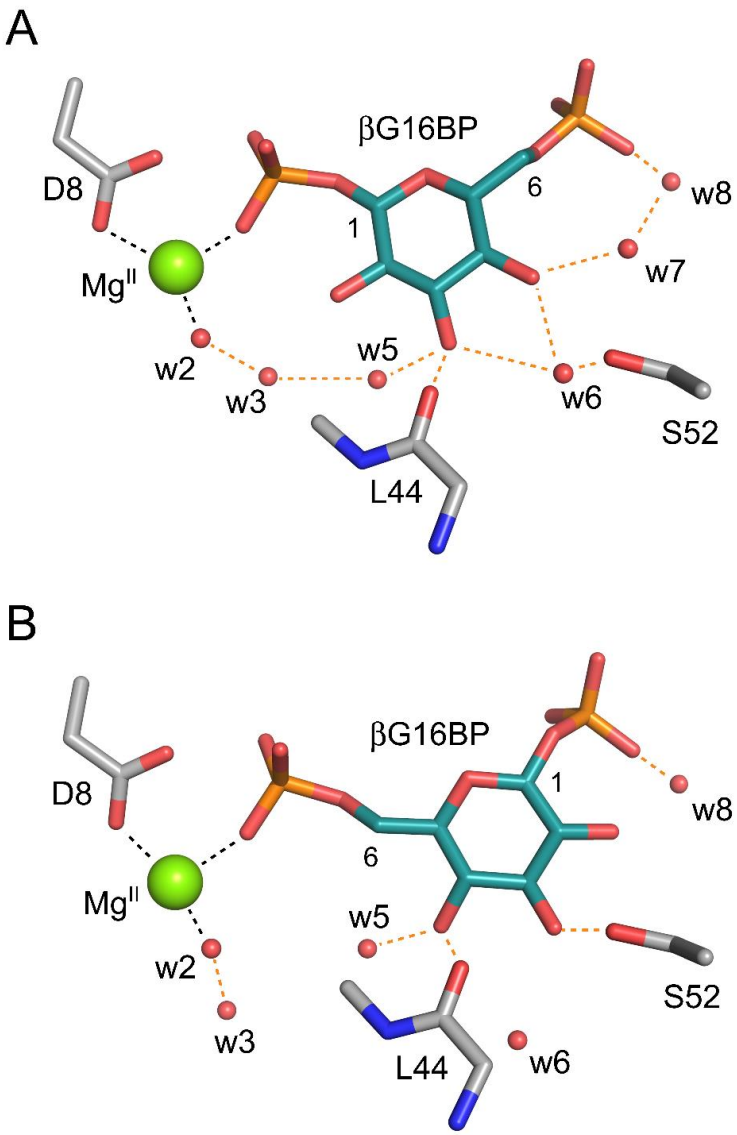

Figure S8. Comparison of βG16BP and structural water coordination in the βPGM$_{D10N}$:βG16BP complexes. The active sites of (A) βPGM$_{D10N}$:P1G6P complex (PDB 5OK1) and (B) βPGM$_{D10N}$:P6G1P complex (PDB 5OK0). Selected residues and the βG16BP ligand are shown as sticks in standard CPK colors, with structural waters (red) and the catalytic Mg^{II} ion (green) drawn as spheres. Orange dashes indicate hydrogen bonds and black dashes show catalytic Mg^{II} ion coordination.

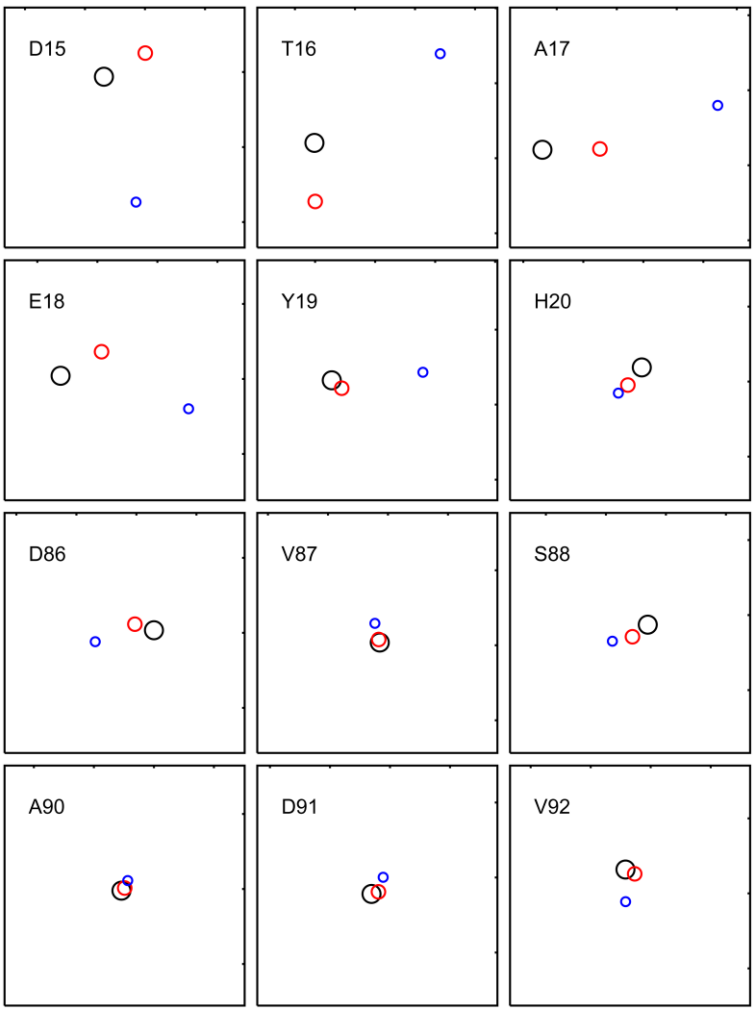

Figure S9. Comparison of backbone amide group peak positions in $^{1}H^{15}N$ TROSY spectra of βPGM_{D10N} complexes. $^{1}H^{15}N$ TROSY peak positions are shown for twelve hinge residues (D15, T16, A17, E18, Y19, H20, D86, V87, S88, A90, D91, V92) of the open βPGM_{D10N}:BeF_3 complex (black circle), the Mg^{II}-bound βPGM_{D10N}:βP1G6P complex (red circle) and the fully closed βPGM_{D10N}:AlF_4:G6P TSA complex (blue circle). The chemical shifts of these hinge residues are sensitive to the degree of closure of the cap and core domains and apart from D15 and T16, the $^{1}H^{15}N$ TROSY peaks of the Mg^{II}-bound βPGM_{D10N}:βP1G6P complex lie in an intermediate position between those of the open βPGM_{D10N}:BeF_3 complex and the fully closed βPGM_{D10N}:AlF_4:G6P TSA complex. These results indicate that the Mg^{II}-bound βPGM_{D10N}:βP1G6P complex is partially open in agreement with the crystal structures. Residues D15 and T16 do not follow this pattern and the crystal structures indicate that these residues play a crucial role in governing optimal hydrogen bonding for substrate coordination by positioning of the general acid–base and closure of the domains through rotation in backbone dihedral angles, which will be different in each of the complexes. For each panel, the x-axis

denotes the backbone amide proton ($^{1}H_{N}$) frequency, with a range of 2 ppm and the y-axis denotes the backbone amide nitrogen (^{15}N) frequency, with a range of 16 ppm. For the βPGM_{D10N}:BeF_3 complex, the $^{1}H_{N}$ and ^{15}N chemical shifts are (in ppm): D15 (8.34, 120.31), T16 (8.84, 113.98), A17 (9.12, 128.97), E18 (9.31, 119.79), Y19 (7.36, 118.38), H20 (8.01, 119.06), D86 (7.35, 114.83), V87 (7.07, 124.81), S88 (9.15, 125.64), A90 (7.77, 120.11), D91 (8.15, 116.09) and V92 (7.21, 123.41). For the Mg^{II}-bound βPGM_{D10N}:βP1G6P complex, the $^{1}H_{N}$ and ^{15}N chemical shifts are (in ppm): D15 (8.00, 118.73), T16 (8.83, 117.88), A17 (8.64, 128.91), E18 (8.97, 118.19), Y19 (7.28, 118.91), H20 (8.13, 120.23), D86 (7.51, 114.42), V87 (7.08, 124.61), S88 (9.28, 126.44), A90 (7.74, 119.94), D91 (8.10, 115.95) and V92 (7.13, 123.70). For the βPGM_{D10N}:AlF_4:G6P TSA complex, the $^{1}H_{N}$ and ^{15}N chemical shifts are (in ppm): D15 (8.07, 128.67), T16 (7.79, 108.03), A17 (7.66, 126.01), E18 (8.24, 121.99), Y19 (6.60, 117.84), H20 (8.21, 120.77), D86 (7.84, 115.59), V87 (7.11, 123.54), S88 (9.45, 126.74), A90 (7.72, 119.44), D91 (8.06, 114.98) and V92 (7.21, 125.55).

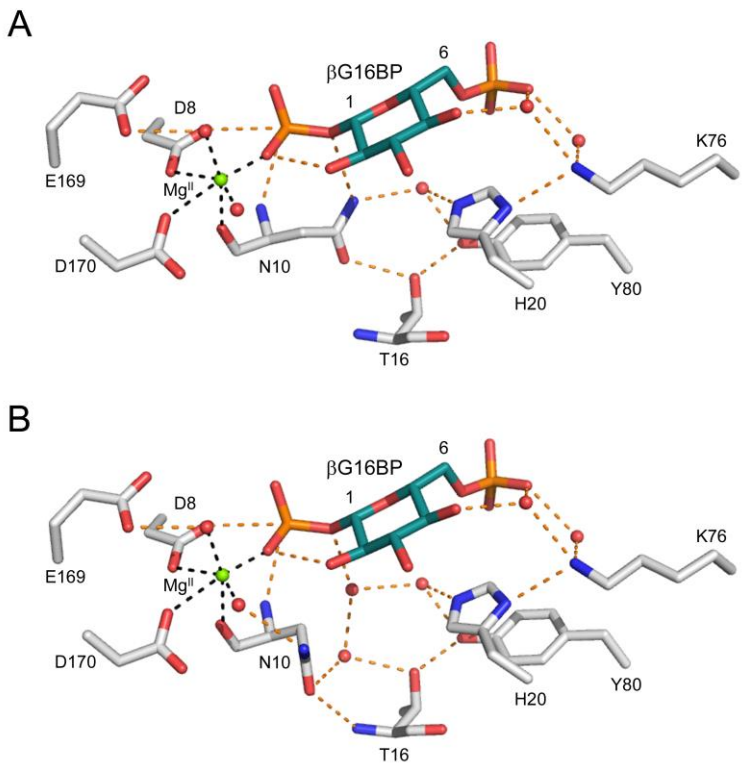

Figure S10. A model showing a potential mechanism for mutase activity in βPGM_{D10N}. Selected active site residues and ligands are shown as sticks in standard CPK colors, with structural waters (red) and the catalytic Mg^{II} ion (green) drawn as spheres. Orange dashes indicate hydrogen bonds and black dashes show metal ion coordination. (A) The βPGM_{D10N}:βP1G6P complex (PDB 5OK1; Figure 3B) with residue N10, the mimic of the protonated form of the general acid–base in the *in* position. The active site arrangement is analogous to that present in the copurified βPGM_{D10N}:βP1G6P complex (PDB 5O6P; Figure 3D). (B) A model of the βPGM_{D10N}:βP1G6P complex with N10 in the *out* position. In this model, the carbonyl oxygen atom of the carboxamide group of N10 forms a hydrogen bond to the amide group of T16, as observed in the βPGM_{D10N}:BeF_3 complex (PDB 5OJZ). Two water molecules which occupy the position of the general acid–base side chain when in the *in* position, comprise part of an extended hydrogen bonded network in the active site involving residues H20, K76, Y80, the phosphate group in the *distal* site, as well as structural and bulk water molecules. Any one of these groups could facilitate proton transfer to the bridging oxygen atom of the transferring phosphoryl group, allowing catalysis to occur in βPGM_{D10N}. The model was prepared by rotation of the N10 side chain and the addition of two water molecules in the active site of the PDB 5OK1 structure. Geometry was optimized against the existing electron density in COOT[42].

Table S1.

Data collection and data processing statistics for the βPGM_{D10N} complexes

Complex	**βPGM_{D10N}:BeF_3**	**βPGM_{D10N}:P1G6P**	**Copurified βPGM_{D10N}:P1G6P**	**βPGM_{D10N}:P6G1P**	**βPGM_{D10N}:AlF_4:G6P**	**βPGM_{D10N}:AlF_4:H_2O:βG1P**
PDB code	PDB 5OJZ	PDB 5OK1	PDB 5O6P	PDB 5OK0	PDB 5OK2	PDB 5O6R
Crystallization conditions	0.6 mM substrate-free βPGM_{D10N} 5 mM $BeCl_2$ 15 mM NaF	0.6 mM substrate-free βPGM_{D10N} 15 mM βG1P, 5 mM $BeCl_2$ 15 mM NaF	0.6 mM copurified βPGM_{D10N}:P1G6P	0.6 mM substrate-free βPGM_{D10N} 15 mM βG1P, 5 mM $BeCl_2$ 15 mM NaF	0.6 mM substrate-free βPGM_{D10N} 10 mM G6P, 5 mM $AlCl_3$ 20 mM NaF	0.6 mM copurified βPGM_{D10N}:P1G6P 5 mM βG1P, 2 mM $AlCl_3$ 10 mM NH_4F
Crystal morphology	Thin plate crystals	Rod shaped crystals	Small needle crystals	Rod shaped crystals	Thin plate crystals	Large plate crystals
Wavelength (Å) **Beamline, Facility**	0.97625 Beamline i03, DLS	0.97950 Beamline i04, DLS	0.933 Beamline ID14-2, ESRF	0.97950 Beamline i04, DLS	0.97625 Beamline i03, DLS	0.933 Beamline ID14-2, ESRF
Space group	$P2_12_12_1$	$P2_12_12_1$	$P2_12_12_1$	$P2_12_12_1$	$P2_12_12_1$	$P2_12_12_1$
Cell dimensions: **a, b, c (Å)** **α, β, γ (°)**	 52.8, 53.8, 81.6 90.0, 90.0, 90.0	 36.7, 74.5, 78.6 90.0, 90.0, 90.0	 31.8, 68.3, 83.2 90.0, 90.0, 90.0	 36.8, 54.9, 103.3 90.0, 90.0, 90.0	 37.5, 54.3, 104.7 90.0, 90.0, 90.0	 36.3, 54.9, 107.6 90.0, 90.0, 90.0
Resolution (Å) [1]	44.3 – 1.3 (1.33 – 1.30)	39.3 – 1.86 (1.91 – 1.86)	20.0 – 2.2 (2.26 – 2.20)	48.5 – 2.15 (2.21 – 2.15)	54.3 – 1.1 (1.12 – 1.10)	20.0 – 1.36 (1.40 – 1.36)
R_{merge} [1,2]	0.05 (0.93)	0.06 (1.90)	0.08 (0.27)	0.31 (1.50)	0.07 (1.03)	0.08 (0.27)
R_{pim} [1]	0.023 (0.542)	0.018 (0.558)	0.052 (0.167)	0.148 (0.721)	0.029 (0.572)	0.018 (0.077)
CC-half [1]	0.999 (0.489)	1.000 (0.599)	–	0.980 (0.391)	0.999 (0.484)	–
$\langle I/\sigma(I) \rangle$ [1]	16.1 (1.3)	25.8 (1.2)	10.0 (4.0)	5.3 (1.2)	12.5 (1.2)	24.5 (7.4)
Completeness (%) [1]	99.0 (88.3)	100.0 (99.9)	98.2 (99.5)	100.0 (100.0)	99.5 (91.6)	93.6 (91.3)
Multiplicity [1]	6.8 (4.4)	12.9 (13.3)	3.3 (3.3)	6.2 (6.4)	6.8 (4.7)	3.0 (2.8)
Total reflections	388282	242890	–	74044	591468	–
Unique reflections	57228	18807	31189	11990	87229	43148
Molecular replacement model	PDB 2WFA	PDB 2WF5	PDB 1O08	PDB 2WF5	PDB 2WF6	PDB 1O08

[1] Values for the higher resolution shell are in parenthesis

[2] $R_{merge} = \sum_h \sum_i |I(h) - I(h)_i| / \sum_h \sum_i I(h)_i$, where I(h) is the mean weighted intensity after rejection of outliers

Table S1 continued.

Refinement statistics for the βPGM$_{D10N}$ complexes

Complex	**βPGM$_{D10N}$:BeF$_3$**	**βPGM$_{D10N}$:P1G6P**	**Copurified βPGM$_{D10N}$:P1G6P**	**βPGM$_{D10N}$:P6G1P**	**βPGM$_{D10N}$:AlF$_4$:G6P**	**βPGM$_{D10N}$:AlF$_4$:H$_2$O:βG1P**
PDB code	PDB 5OJZ	PDB 5OK1	PDB 5O6P	PDB 5OK0	PDB 5OK2	PDB 5O6R
***R* (%) [3] / R_{free} (%) [4]**	13.6 / 17.0	19.8 / 24.6	19.5 / 24.8	22.0 / 29.2	14.8 / 17.0	10.7 / 14.6
Number of atoms:						
Protein	1724	1688	1611	1680	1812	1690
Ligands	4	20	20	20	21	21
Metal ions	2	1	1	1	3	2
Water	246	67	70	84	244	379
Protein residues	218	218	209	218	218	218
RMS deviations:						
Bonds (Å)	0.014	0.011	0.024	0.012	0.010	0.024
Angles (°)	1.48	1.49	2.39	1.50	1.47	2.15
Average B factors (Å^2):	20.44	42.68	39.63	31.86	15.41	15.01
Main chain	16.30	41.23	39.02	30.54	12.63	10.64
Side chains	20.83	44.75	41.39	33.62	15.40	14.15
Ligands	13.74	35.43	27.16	32.29	8.67	7.62
Metal ions	24.35	37.50	23.43	46.62	15.18	16.48
Water	32.26	38.77	31.28	28.34	25.91	27.33
Ramachandran analysis:						
Favored/allowed (%)	98.6	95.8	94.2	97.7	97.7	97.2
Disallowed (%)	0.0	0.5	0.5	0.0	0.0	0.0
MolProbity score	0.69 (100th percentile)	1.11 (100th percentile)	2.62 (41st percentile)	1.12 (100th percentile)	1.11 (96th percentile)	1.17 (97th percentile)

[3] $R = \sum_{hkl} \left| |F_{obs}| - k|F_{calc}| \right| \Big/ \sum_{hkl} |F_{obs}|$, where F_{obs} and F_{calc} are the observed and calculated structure factor amplitudes

[4] $R_{free} = \sum_{hkl \subset T} \left| |F_{obs}| - k|F_{calc}| \right| \Big/ \sum_{hkl \subset T} |F_{obs}|$, where F_{obs} and F_{calc} are the observed and calculated structure factor amplitudes and T is the test set of data omitted from refinement (5% in this case)

Table S2.
Pairwise cap domain rotations calculated using DynDom for selected βPGM complexes

βPGM complex	**βPGM complex**	**Cap domain rotation (°)** [1]	**Cap domain translation (Å)** [2]
$βPGM_{WT}$ (PDB 2WHE)	$βPGM_{WT}$:MgF_3:G6P (PDB 2WF5)	35.0	1.4
$βPGM_{WT}$:BeF_3 (PDB 2WFA)	$βPGM_{WT}$:MgF_3:G6P (PDB 2WF5)	35.5	1.5
$βPGM_{D10N}$:BeF_3 (PDB 5OJZ)	$βPGM_{WT}$:BeF_3 (PDB 2WFA)	5.9	0.0
$βPGM_{D10N}$:P1G6P (PDB 5OK1)	$βPGM_{WT}$:MgF_3:G6P (PDB 2WF5)	13.2	–0.8
Copurified $βPGM_{D10N}$:P1G6P (PDB 5O6P)	$βPGM_{WT}$:MgF_3:G6P (PDB 2WF5)	13.5	–0.6
$βPGM_{D10N}$:P6G1P (PDB 5OK0)	$βPGM_{WT}$:MgF_3:G6P (PDB 2WF5)	14.0	–1.0
$βPGM_{D10N}$:AlF_4:G6P (PDB 5OK2)	$βPGM_{WT}$:MgF_3:G6P (PDB 2WF5)	No dynamic domains found	No dynamic domains found
$βPGM_{D10N}$:AlF_4:H_2O:βG1P (PDB 5O6R)	$βPGM_{WT}$:MgF_3:G6P (PDB 2WF5)	14.1	–1.0
$βPGM_{D10N}$:AlF_4:H_2O:βG1P (PDB 5O6R)	$βPGM_{WT}$:MgF_3:β$G1CF_SP$ (PDB 4C4S) [3]	14.2	–1.1
$βPGM_{D10N}$:AlF_4:G6P (PDB 5OK2)	$βPGM_{D10N}$:AlF_4:H_2O:βG1P (PDB 5O6R)	13.8	–0.9
$βPGM_{D10N}$:P1G6P (PDB 5OK1)	$βPGM_{D10N}$:AlF_4:G6P (PDB 5OK2)	13.0	–0.8
Copurified $βPGM_{D10N}$:P1G6P (PDB 5O6P)	$βPGM_{D10N}$:AlF_4:G6P (PDB 5OK2)	13.4	–0.5
$βPGM_{D10N}$:P6G1P (PDB 5OK0)	$βPGM_{D10N}$:AlF_4:G6P (PDB 5OK2)	13.7	–0.9
$βPGM_{D10N}$:P1G6P (PDB 5OK1)	Copurified $βPGM_{D10N}$:P1G6P (PDB 5O6P)	5.2	–0.3
$βPGM_{D10N}$:P6G1P (PDB 5OK0)	Copurified $βPGM_{D10N}$:P1G6P (PDB 5O6P)	8.3	–0.4
$βPGM_{D10N}$:P1G6P (PDB 5OK1)	$βPGM_{D10N}$:P6G1P (PDB 5OK0)	3.4	–0.1

[1] Hinge located at T16 for all pairwise comparisons

[2] DynDom translation term was less than ± 1.5 Å for all pairwise comparisons and so was not included in the text

[3] Where β$G1CF_SP$ corresponds to the α-fluorophosphonate analogue of β-glucose 1-phosphate[19]